Hindawi
Advances in Materials Science and Engineering
Volume 2021, Article ID 5907292, 11 pages
https://doi.org/10.1155/2021/5907292

Research Article

Microstructure and Performances for Wear-Resistant Steel through the WAAM Technology

Meng Ying,[1] Chun Guo ,[1] Yun Li,[1] Tai Yu Kang,[1] Wu Meng Liu,[2] and Sui Song Wu[2]

[1]*College of Mechanical Engineering, Anhui Science and Technology University, Bengbu 233000, China*
[2]*College of Mechanical Engineering, Anhui Polytechnic University, Wuhu 241000, China*

Correspondence should be addressed to Chun Guo; guochun@ahstu.edu.cn

Received 11 May 2021; Revised 7 September 2021; Accepted 21 October 2021; Published 26 November 2021

Academic Editor: Ling B. Kong

This work describes the wire arc additive manufacturing (WAAM) approach used to fabricate parts from wear-resistant steel. The microstructure, crystal structures, and mechanical properties of the resulting samples were thoroughly analyzed. The wear-resistant steel parts demonstrated good forming, no internal defects, good metallurgical bonding, and excellent wear resistance. The metallographic analysis confirmed that the main phase was ferrite. The microhardness of the sample along its cross section was uniform in both horizontal and vertical directions and equals to 464.7$HV_{0.2}$ and 482.4 $HV_{0.2}$, respectively. The average values of tensile strength, elongation ratio, and room temperature Charpy shock were equal to 945.3 MPa, 4.3%, and 5 J, respectively.

1. Introduction

WAAM, similar to 3D printing technology, uses the heat generated by the arc to provide a heat source during work to melt the metal wire. The melted metal wire will follow the set forming path to melt the metal slurry. On the substrate, the molten slurry is piled up layer by layer, and it is cooled and formed until it becomes a metal part. Therefore, almost any complex shape of metal parts can be produced [1–8]. This method has several advantages over traditional manufacturing methods such as environmental friendliness, high material utilization, and molding efficiency, as well as low manufacturing costs [9–14]. 3D printing is especially popular for applications related to biomedicine, shipbuilding, aerospace, mold production, and automobile manufacturing. WAAM uses an electric arc as a heat source and filler wires as raw materials. It is suitable for manufacturing large parts [15–21] especially for agricultural machinery prone to corrosion and wear after prolonged usage. As a result, wearable parts such as pins need to be replaced frequently, which is not economically feasible.

Wear is one of the primary forms of parts' failure. It consumes significant energy and wastes raw materials. Approximately 30–50% of the mechanical energy is consumed by friction and wear. Statistics provided by the German Federal Ministry of Technology and Science assessed that wear and tear cause 5 billion euros of losses [22, 23]. China lacks such statistical data. However, a report provided by the Chinese Machinery Department states that in 1974–1975, the annual steel consumption for auto part production was 230,000 tons, two-thirds of which were used to maintain and repair damages caused by wear. In addition, according to sparse statistical data from Chinese departments of electric power, building materials, metallurgy, coal mining, and agricultural machinery, spare parts' production annually requires over 1.5 million tons of steel. For example, the losses due to the wear of the middle groove of the scraper conveyor used in coal mines account for 100–200 million yuan per year [24–33]. Thus, these and all other economic losses caused by wear and tear of the mechanical equipment and the steel consumption are enormous. However, these damages could be prevented to a certain degree if the quality of the resistant steel (to make it more wear-resistant) is improved. For this purpose, scientists and engineers need to develop new high-performance wear-resistant steel and understand steel wear mechanisms, which will provide desired insights [34–37].

Therefore, the purpose of this work was to compare wear-resistant material used as raw sources for the arc additive manufacturing of the parts, for which excellent wear resistance is required. We studied the structure and mechanical properties of the wear-resistant materials subjected to the WAAM. This paper provides data needed to advance and improve the fabrication of reliable agricultural machinery and equipment. The wear-resistant steel typically contains Si, Mn, Cr, Mo, V, W, Ni, Ti, B, Cu, and rare earth elements. In this paper, we focused on the wear-resistant steel containing high levels of C and Cr.

2. Experimental Procedures

We used the FILLARC DUR 606M 1.2 mm in diameter wire consisting of wear-resistant steel. Its chemical composition is shown in Table 1. The wire arc additive manufacturing (WAAM) equipment used the AIR10 and AIR-TP automated software (see Figure 1). The substrate was a $300 \times 100 \times 10$ mm steel plate, polished prior to the WAAM using a grinding wheel to remove the surface layers to reduce the plate's deformation. The substrate was attached to the base steel plate. Our prior work established the single-layer single-pass and single-layer multipass parameters, which were then used in our present work to obtain the optimum weld bead shapes. The control over the forming accuracy during WAAM was performed by measuring the interlayer temperature using infrared measurements. The sample was $150 \times 20 \times 60$ mm in size. The samples were printed under the 80% Ar/20% CO_2 atmosphere. The interlayer temperature did not rise above 150°C. The interlayer temperature is considered to be one of the most important parameters [38]. The voltage and current were maintained at 19 V and 80 A, respectively. However, the first layer current was 90 A. The sample printing speed was 5 mm/s. All WAAM parameters are given in Table 2.

After the main sample was produced, it was cut into $17 \times 28 \times 20$ mm pieces for further hardness, metallographic X-ray analysis, and scanning electron microscopy (SEM) analysis. The tensile tests were performed on both sample sides parallel and perpendicular to the deposition direction (see Figure 2).

The room temperature tensile tests were performed according to GB/T 228.1-2010 standard using UTM-6104 material testing machine. The displacement control was implemented during sample stretching, which was performed at a 0.005 min^{-1} strain rate. The impact tests used a pendulum impact testing machine (JB-W300A). These measurements were performed at room temperature and for each data point. One sample piece was polished and then etched in ferric nitrate solution in alcohol for further microstructural observations performed according to the GB/T 13298-2015 Metal Microstructure Inspection Method using a 4XC microscope. X-ray diffraction (XRD) performed using the XD-3 instrument was used to determine the phase composition. The analysis parameters were CuK-α emission as an X-ray source, 36 V, 24 A, 2°/min scan speed, 0.02° step, and 10–90° range.

The friction tests were performed using dry and ball-disk frictions. For this purpose, the test sample was placed into a three-jaw fixture, after which the friction ball (6 mm in diameter) was placed onto the sample surface. The sample weight was recorded before the 30 N friction force was applied. Other friction test parameters were 500 rpm spindle speed and 1800 s test time.

SEM was performed by the Zeiss EVO®18 instrument to analyze the sample morphologies after the impact, tensile fracture, and wear tests. For transmission electron microscopy (TEM), performed using the JEM-2100 instrument operated at 200 kV, a 0.5 mm sample slice was ground to ~120 μm. Three disks were punched out of this piece and then ground to 50 μm.

For the double-spray electrolysis tests, performed at −20°C and 75 V using Gatan 691 ion thinner to treat the Ar for 0.5 h, we used 4% perchloric acid solution as the electrolyte. The Vickers microhardness was tested according to GB/T 4340.1-2009 "Metallic material" procedure performed by using the HV-1000Z tester at 200 g force. The starting point of the test was the upper section of the sample 2 mm away from the edge. Twelve points 1 mm apart from each other were tested.

3. Results and Discussion

3.1. Forming Characteristics. 3D printed wear-resistant steel sample is formed without collapsing (see Figure 3) and with small welding wire splash. The cross section analysis of the sample showed minimum defects and satisfactory metallurgical bonding (see Figure 4). These observations further confirmed the excellent formability of the WAAM-printed wear-resistant steel.

3.2. Microstructure and Crystal Structure. Figure 5 shows the metallographic data obtained for different sections (columnar crystal, remelting, and heat-affected zones) of the part fabricated in this work by WAAM. The crystals corresponded to the ferrite phase. The black zigzag features corresponded to the grain boundaries, while the inclusions which appeared as small black particles were metal carbides.

The low-magnification analysis of the sample revealed no cracks, holes, and solid inclusions and only some fusions, incomplete penetration, poorly shaped grains, and other defects. Thus, the internal structure of the wear-resistant steel sample prepared by WAAM was very satisfactory.

XRD of the steel sample prepared by WAAM showed three strong peaks at 43°, 64°, and 80°, corresponding to the α-Fe phase (see Figure 6). No other phases were detected very likely because their contents were below 5%. The SAED confirmed that the crystalline phase in our sample was α-Fe (see Figure 7).

3.3. Mechanical Properties. The microhardness distribution diagram shows that the hardness of the wear-resistant steel samples prepared by WAAM was uniform and in the 410–520 $HV_{0.2}$ range (see Figure 8). The average microhardness values in the transverse and longitudinal directions

Table 1: Chemical composition (in wt%) of the welding wire used in this work for WAAM.

C	Si	Mn	P	S	Cr	Mo
0.71	0.68	1.35	0.011	0.008	6.23	0.58

Figure 1: WAAM experimental system used in this work.

Table 2: WAAM parameters used in this work.

Wire diameter (mm)	Voltage (V)	Current (A)	Wire feed speed (mm/s)	Printing speed (mm/s)	Tip to work distance (mm)	Gas flow (l/min)	Interpass temperature (°C)
1.2	19	80	5	12	10–15	20	≤150

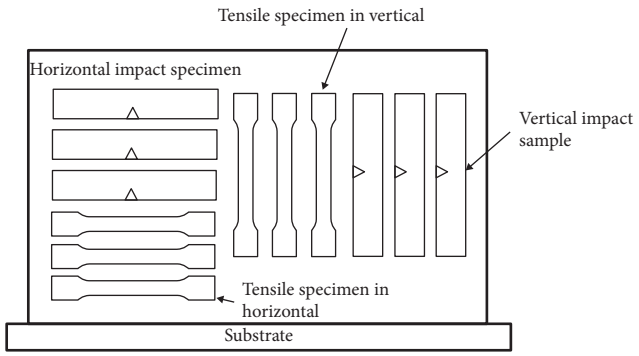

Figure 2: Diagram showing sampling points.

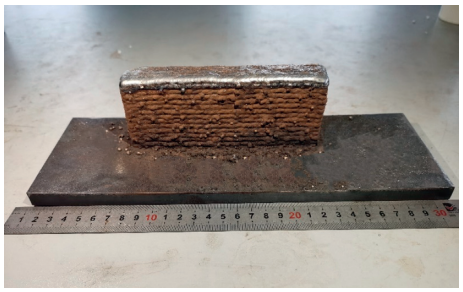

Figure 3: Steel sample prepared in this work by WAAM.

were equal to 464.7HV$_{0.2}$ and 482.4 HV$_{0.2}$, respectively. These values were remarkably close to each other. The microhardness fluctuations were mainly due to the structural

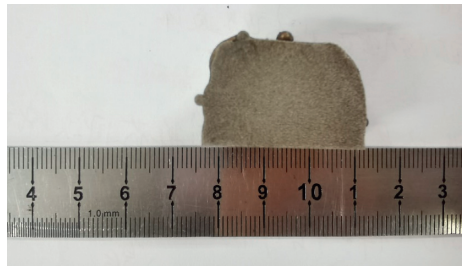

Figure 4: Photograph showing a cross section of the steel sample prepared by WAAM.

variations of the sample; the sample cross section analysis revealed that it possessed multilayer and multipass structure, with the first layer possessing the weld bead structure. Additionally, this first layer was affected by the second one, which also possessed the weld bead structure. The original columnar crystal, remelted, and heat-affected regions were observed because of the thermal cycle of the same-layer weld bead. Their microhardness varied because these regions have different grain sizes and precipitate contents [39, 40].

The mechanical properties of the samples prepared in this work by WAAM were excellent: the average tensile strength, elongation, and room temperature Charpy shock values were equal to 945.3 MPa, 4.3%, and 5 J, respectively (see Table 3).

Microscopical analysis of the tensile fracture of our steel sample revealed no apparent defects (see Figure 9(a)), which agrees with the experimental results shown in Table 3, especially for the samples with lower elongation values.

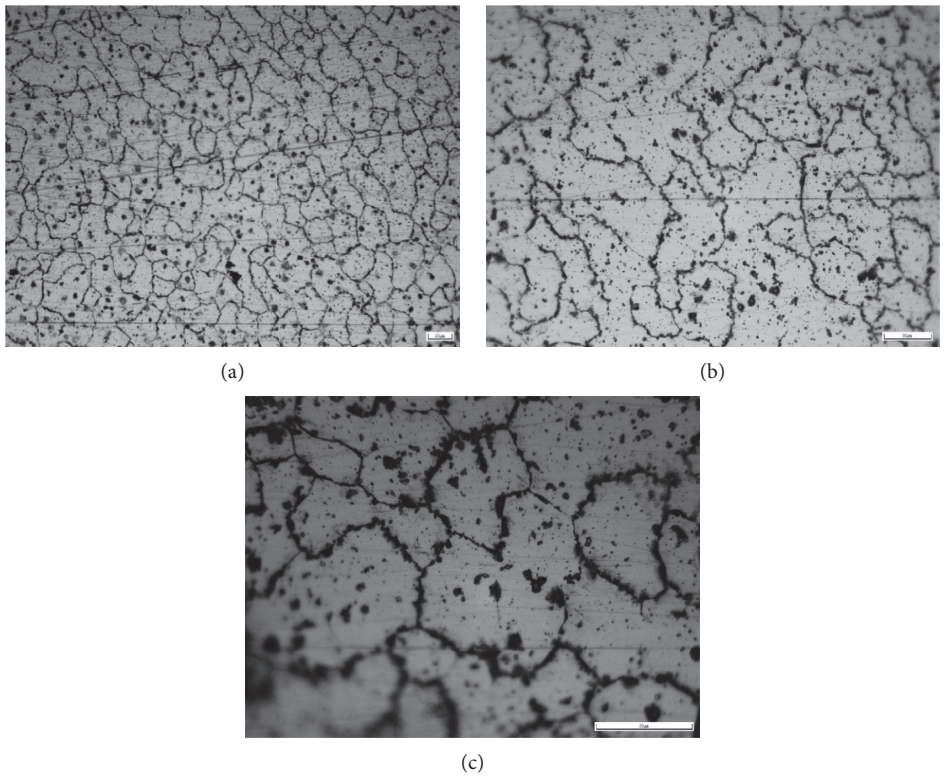

Figure 5: The microstructure of different sample sections at 100 (a), 200 (b), and 400 (c) time magnifications.

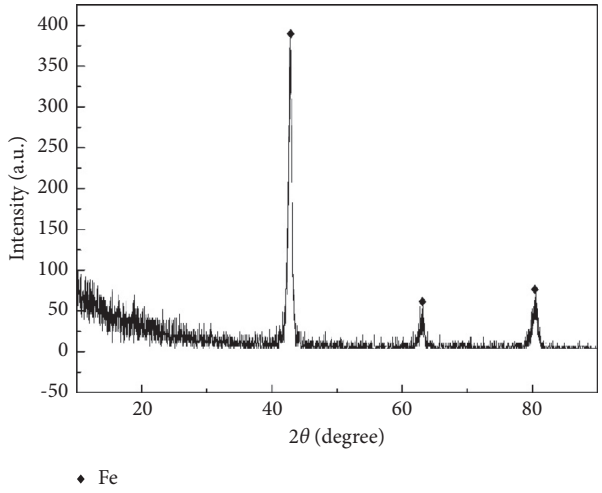

Figure 6: XRD pattern collected for the sample fabricated by WAAM.

Figures 9(b)–9(d) show the morphologies of the tensile fracture of the fibrous, radiation, and shear lip zones, respectively. The fracture was flat and bright, which implies that it was a brittle fracture, the fracture surface of which is usually perpendicular to the tensile stress. The fracture is composed of shiny crystalline surfaces with slight fibrous irregularities. The ratio of the radiation area was larger (see Figure 9) than that of the fibre area. Thus, the material possessed poor toughness and was very brittle.

3.4. Wear Resistance. Figure 10 shows the samples before and after the friction tests. Five sets of friction tests under different loads were performed. The wear conditions were observed, and calculations and analysis results (namely, the mass change and wear rate of the sample before and after the friction tests) are presented in Table 4.

Figure 11 shows the relationship between the wear rate and the load. As the load was increased, the wear rate increased as well.

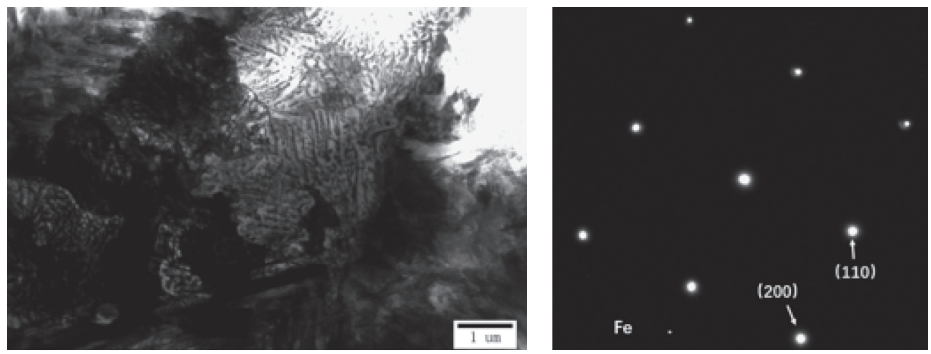

(a) (b)

Figure 7: TEM micrograph of the WAAM-printed sample (a) and the corresponding SAED pattern (b).

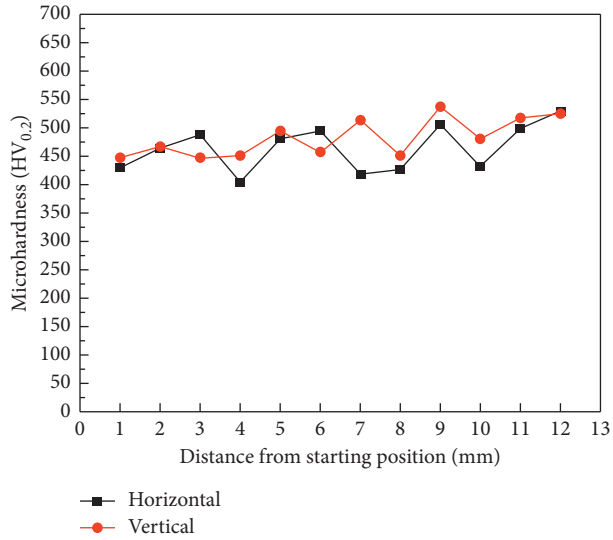

Figure 8: Microhardness distribution of the sample prepared by WAAM.

Table 3: Tensile strength, elongation, and room temperature Charpy shock impact values of the steel samples manufactured by WAAM.

Sample	Tensile strength (MPa)	Elongation (%)	Impact value (J)
1	945.55	4.2	5
2	950.33	4.4	5
3	940.08	4.3	5

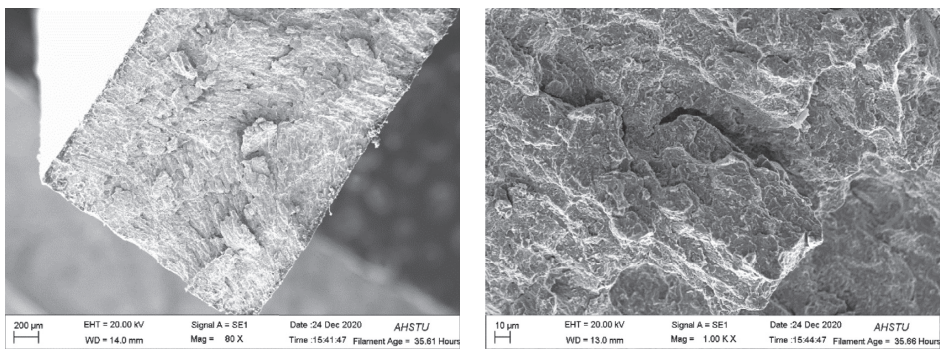

(a) (b)

Figure 9: Continued.

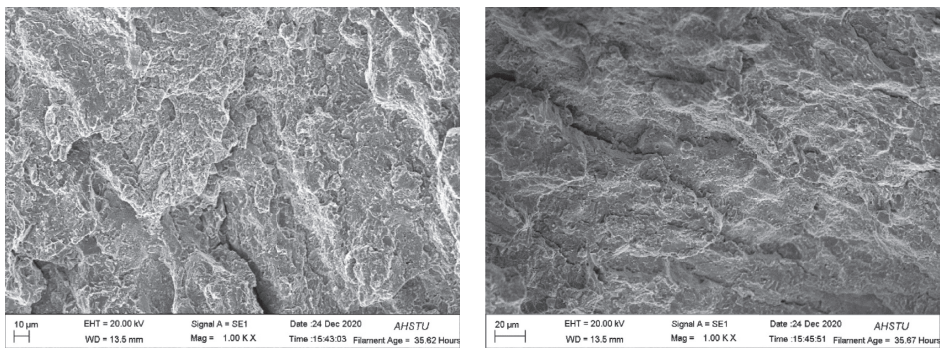

(c) (d)

Figure 9: SEM micrographs showing tensile fracture morphologies: (a) overall fracture appearance; (b) primary fibre zone; (c) radial zone; (d) secondary fibre zone.

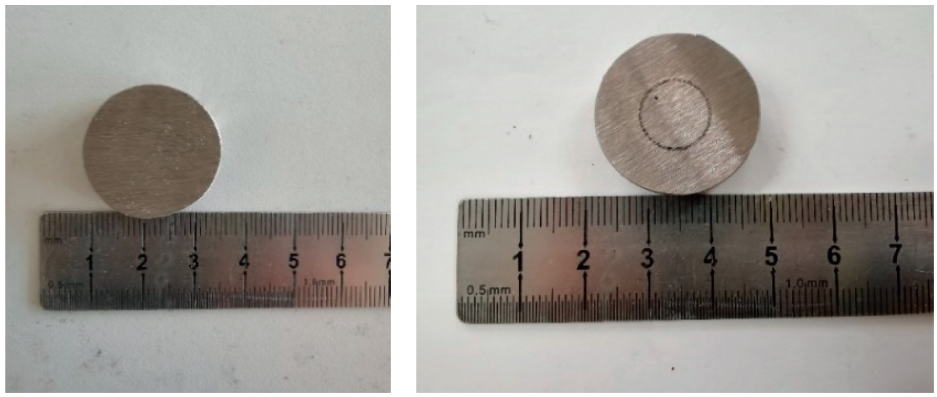

(a) (b)

Figure 10: Photographs showing the sample before (a) and after (b) friction tests.

Table 4: Sample quality and wear rate.

Sample	Load (N)	Sample weight (mg)		Wear rate (mg/(N ∗ mm))
		Before the test	After the test	
1	20	29980.9	29980.4	4.4250×10^{-8}
2	25	27754.4	27753.5	6.3720×10^{-8}
3	30	28549.9	28546.7	1.8880×10^{-7}
4	35	27351.4	27347.6	1.9217×10^{-7}
5	40	29420.5	29415.3	2.3010×10^{-7}

The relationship between friction coefficient and time (shown in Figure 12) revealed that as the load was increased, the friction coefficient and the wear rate also increased.

SEM of the sample subjected to the friction tests showed numerous groove-shaped wear marks along a fixed direction (see Figure 13). The surface of the material also demonstrated some spalling pits formed due to the abrasive and adhesive wear.

Continuous long strip furrows appeared on the worn surface, which is typical for abrasive wear. The depth of these furrows corresponds to the severity of the wear. In our case, the worn surface was relatively smooth, with only minor cracks. As the load force was increased, the wear rate increased and was on the 10^{-7} order of magnitude. Thus, the material possessed excellent wear resistance, especially at higher loads.

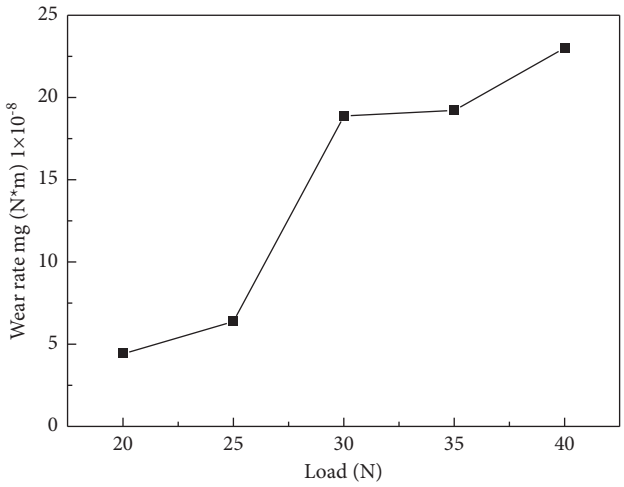

Figure 11: The relationship between the load and the wear rate.

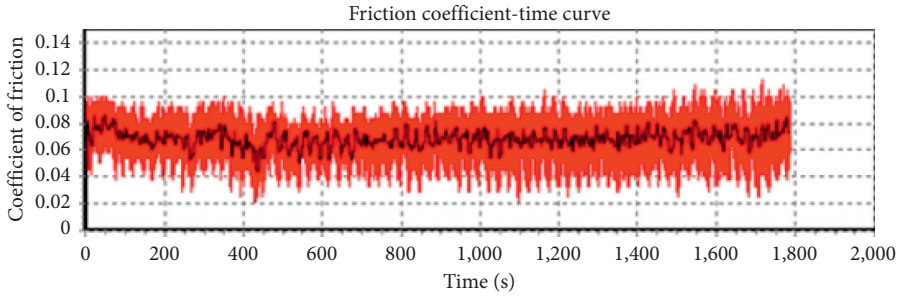

(a)

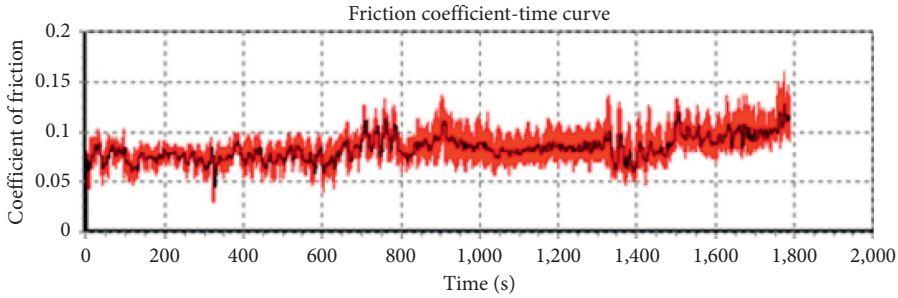

(b)

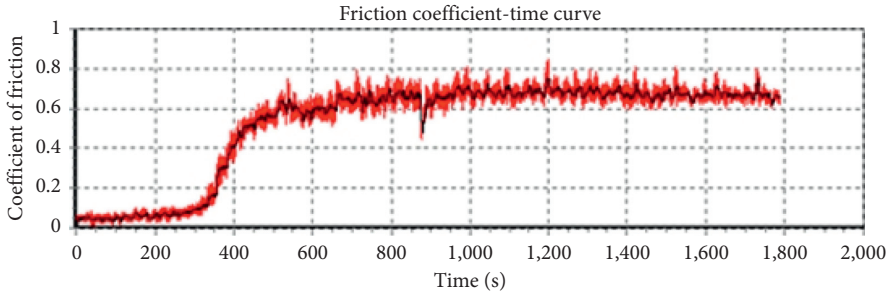

(c)

Figure 12: Continued.

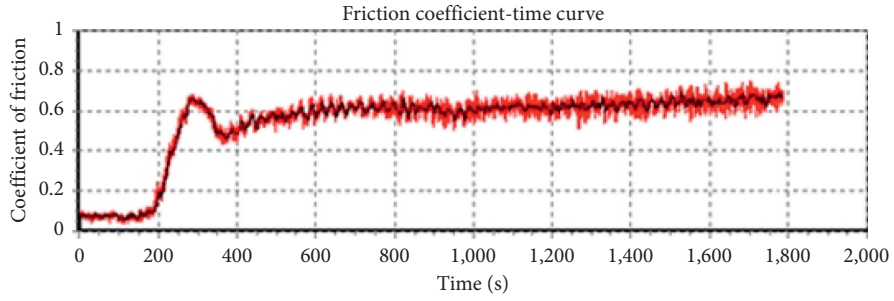

(d)

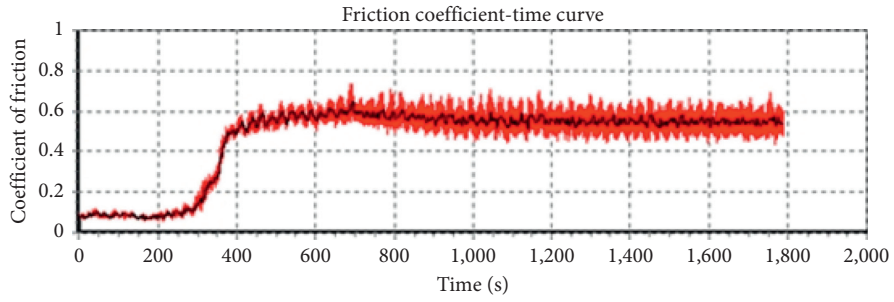

(e)

Figure 12: The relationship between friction coefficient and time under different loads: (a) 20 N, (b) 25 N, (c) 30 N, (d) 35 N, and (e) 40 N.

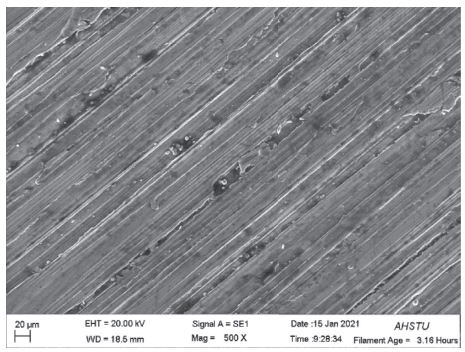

(a)

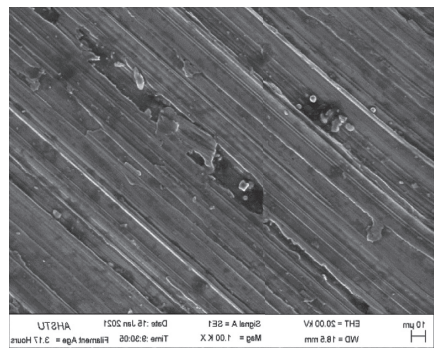

(b)

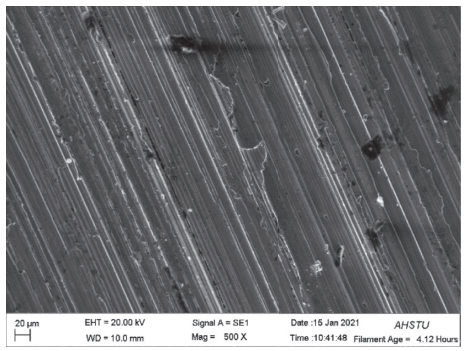

(c)

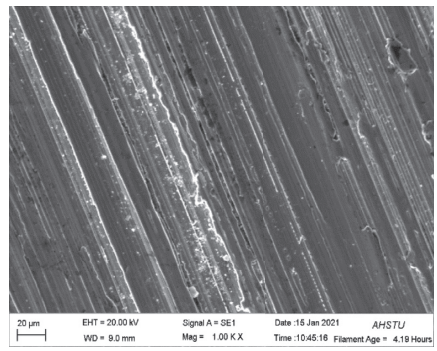

(d)

Figure 13: Continued.

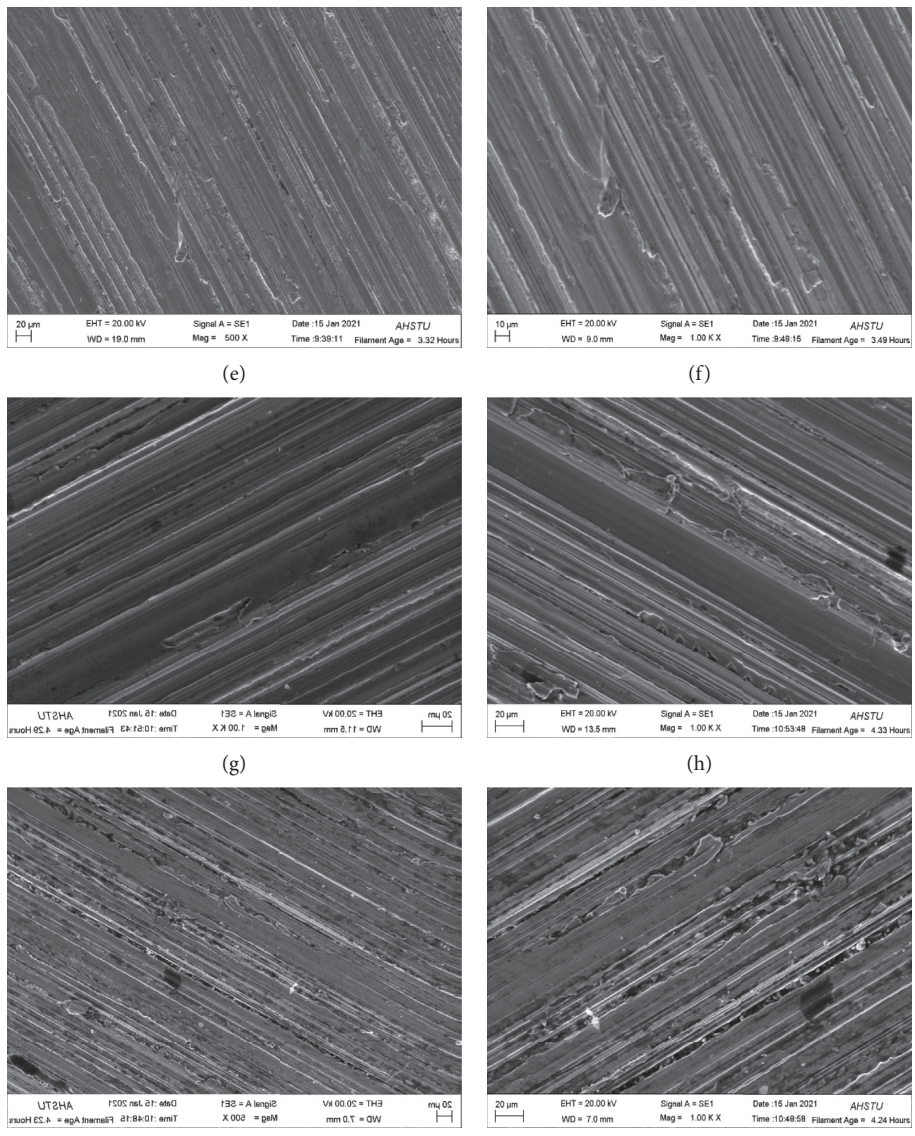

Figure 13: Morphology of the sample at 500 (a, c, e, g, i) and 1000 (b, d, f, h, j) times magnifications subjected to wear tests at (a, b) 20 N, (c, d)25 N, (e, f) 30 N, (g, h) 35 N, and (i, j) 40 N loads.

4. Conclusions

The wear-resistant steel samples were fabricated by wire arc additive manufacturing (WAAM). The resulting samples possessed excellent forming properties and no significant defects. The internal metallurgical bondings of the samples were very satisfactory. The microhardness values in the transverse and longitudinal directions were very similar, with the average values equal to 464.7 $HV_{0.2}$ and 482.4 $HV_{0.2}$, respectively. The samples also possessed excellent mechanical properties: their average tensile strength, elongation, and room temperature Charpy shock values were equal to 945.3 MPa, 4.3%, and 5 J, respectively. We also observed excellent friction resistance of these steel-resistant parts. The results obtained in this work deliver insights into the theoretical and experimental understanding of WAAM for fabricating wear-resistant steel parts for agricultural machinery.

Data Availability

The data used to support this study are available from the corresponding author upon request.

Conflicts of Interest

The authors declare that there are no conflicts of interest.

Acknowledgments

This research was supported by the Collaborative Innovation Program for College Students in Anhui Province, the Natural Science Foundation of Anhui Province, and the Talent Program of Anhui University of Science and Technology under the grant numbers GXXT-2019-022, 1908085QE174, and RCYJ201905, respectively.

References

[1] C. Gao, X. Chen, C. Su, and X. Chen, "Location dependence of microstructure and mechanical properties on wire arc additively manufactured nuclear grade steel," *Vacuum*, vol. 168, Article ID 108818, 2019.

[2] V. Laghi, M. Palermo, G. Gasparini, V. A. Girelli, and T. Trombetti, "Experimental results for structural design of Wire-and-Arc Additive Manufactured stainless steel members," *Journal of Constructional Steel Research*, vol. 167, Article ID 105868, 2020.

[3] Y. Guo, G. Quan, Y. Jiang, L. Ren, L. Fan, and H. Pan, "Formability, microstructure evolution and mechanical properties of wire arc additively manufactured AZ80M magnesium alloy using gas tungsten arc welding," *Journal of Magnesium and Alloys*, vol. 9, no. 1, 2020.

[4] V. T. Le, D. S. Mai, and Q. H. Hoang, "Effects of cooling conditions on the shape, microstructures, and material properties of SS308L thin walls built by wire arc additive manufacturing," *Materials Letters*, vol. 280, Article ID 128580, 2020.

[5] Q. Shen, X. Kong, X. Chen, X. Yao, B. Deev Vladislav, and S. Prusov Evgeny, "Powder plasma arc additive manufactured CoCrFeNi(SiC)x high-entropy alloys: microstructure and mechanical properties," *Materials Letters*, vol. 282, Article ID 128736, 2021.

[6] J. G. Lopes, C. M. Machado, V. R. Duarte, T. A. Rodrigues, T. G. Santos, and J. P. Oliveira, "Effect of milling parameters on HSLA steel parts produced by Wire and Arc Additive Manufacturing (WAAM)," *Journal of Manufacturing Processes*, vol. 59, pp. 739–749, 2020.

[7] Z. Zeng, B. Q. Cong, J. P. Oliveira et al., "Wire and arc additive manufacturing of a Ni-rich NiTi shape memory alloy: microstructure and mechanical properties," *Additive Manufacturing*, vol. 32, Article ID 101051, 2020.

[8] T. A. Rodrigues, V. R. Duarte, D. Tomás et al., "In-situ strengthening of a high strength low alloy steel during Wire and Arc Additive Manufacturing (WAAM)," *Additive Manufacturing*, vol. 34, Article ID 101200, 2020.

[9] P. C. Priarone, E. Pagone, F. Martina, A. R. Catalano, and L. Settineri, "Multi-criteria environmental and economic impact assessment of wire arc additive manufacturing," *CIRP Annals-Manufacturing Technology*, vol. 69, no. 1, 2020.

[10] B. Matteo, L. Vittoria, and T. Tomaso, "Simultaneous design of the topology and the build orientation of Wire-and-Arc Additively Manufactured structural elements," *Computers & Structures*, vol. 242, no. 5, 2021.

[11] Y. Ma, Z. Hu, Y. Tang et al., "Laser opto-ultrasonic dual detection for simultaneous compositional, structural, and stress analyses for wire + arc additive manufacturing," *Additive Manufacturing*, vol. 31, Article ID 100956, 2020.

[12] D. Michl, S. Benjamin, and M. Bambach, "Ring rolling of preforms made by wire-arc additive manufacturing," *Procedia Manufacturing*, vol. 47, pp. 342–348, 2020.

[13] Z. Qiu, B. Wu, H. Zhu et al., "Microstructure and mechanical properties of wire arc additively manufactured Hastelloy C276 alloy," *Materials & Design*, vol. 195, Article ID 109007, 2020.

[14] L. Yuan, Z. Pan, D. Ding et al., "Investigation of humping phenomenon for the multi-directional robotic wire and arc additive manufacturing," *Robotics and Computer-Integrated Manufacturing*, vol. 63, Article ID 101916, 2020.

[15] Z. Li, C. Liu, T. Xu et al., "Reducing arc heat input and obtaining equiaxed grains by hot-wire method during arc additive manufacturing titanium alloy," *Materials Science and Engineering A*, vol. 742, pp. 287–294, 2019.

[16] L. Wang, J. Xue, and Q. Wang, "Correlation between arc mode, microstructure, and mechanical properties during wire arc additive manufacturing of 316L stainless steel," *Materials Science and Engineering A*, vol. 751, pp. 183–190, 2019.

[17] S. Chandrasekaran, S. Hari, and M. Amirthalingam, "Wire arc additive manufacturing of functionally graded material for marine risers," *Materials Science and Engineering A*, vol. 792, no. C, Article ID 139530, 2020.

[18] C. Wang, T. G. Liu, P. Zhu, Y. H. Lu, and T. Shoji, "Study on microstructure and tensile properties of 316L stainless steel fabricated by CMT wire and arc additive manufacturing," *Materials Science and Engineering A*, vol. 796, Article ID 140006, 2020.

[19] D. Raimundi Corradi, A. Q. Bracarense, B. Wu, D. Cuiuri, Z. Pan, and H. Li, "Effect of Magnetic Arc Oscillation on the geometry of single-pass multi-layer walls and the process stability in wire and arc additive manufacturing," *Journal of Materials Processing Technology*, vol. 283, Article ID 116723, 2020.

[20] P. Wang, H. Zhang, H. Zhu, Q. Li, and M. Feng, "Wire-arc additive manufacturing of AZ31 magnesium alloy fabricated by cold metal transfer heat source: processing, microstructure, and mechanical behavior," *Journal of Materials Processing Technology*, vol. 288, Article ID 116895, 2021.

[21] Y. Xiong, A. G. Dharmawan, Y. Tang, S. Foong, G. S. Soh, and D. W. Rosen, "A knowledge-based process planning framework for wire arc additive manufacturing," *Advanced Engineering Informatics*, vol. 45, no. C, Article ID 101135, 2020.

[22] T. Yuan, Z. Yu, S. Chen, M. Xu, and X. Jiang, "Loss of elemental Mg during wire + arc additive manufacturing of Al-Mg alloy and its effect on mechanical properties," *Journal of Manufacturing Processes*, vol. 49, pp. 456–462, 2020.

[23] J. Huang, Y. Wen, S. Yu, L. Zhang, X. Yu, and D. Fan, "Droplet transfer behavior in bypass-coupled wire arc additive manufacturing," *Journal of Manufacturing Processes*, vol. 49, pp. 397–412, 2020.

[24] T. He, S. Yu, Y. Shi, and A. Huang, "Forming and mechanical properties of wire arc additive manufacture for marine propeller bracket," *Journal of Manufacturing Processes*, vol. 52, pp. 96–105, 2020.

[25] B. Michalis, C. Davide, and P. Alin, "Current mode effects on weld bead geometry and heat affected zone in pulsed wire arc additive manufacturing of Ti-6-4 and Inconel 718," *Journal of Manufacturing Processes*, vol. 60, pp. 61–74, 2020.

[26] P. Kumar and N. K. Jain, "Effect of material form on deposition characteristics in micro-plasma transferred arc additive manufacturing process," *CIRP Journal of Manufacturing Science and Technology*, vol. 30, pp. 195–205, 2020.

[27] H. P. N. Nagarajan, S. Panicker, H. Mokhtarian, E. Coatanéa, and K. R. Haapala, "Improving worker health and safety in wire arc additive manufacturing: a graph-based approach," *Procedia CIRP*, vol. 90, pp. 461–466, 2020.

[28] A. U. Khan and Y. K. Madhukar, "An economic design and development of the wire arc additive manufacturing setup," *Procedia CIRP*, vol. 91, pp. 182–187, 2020.

[29] Y. Zhao, Y. Jia, S. Chen, J. Shi, and F. Li, "Process planning strategy for wire-arc additive manufacturing: thermal behavior considerations," *Additive Manufacturing*, vol. 32, Article ID 100935, 2020.

[30] A. V. Nemani, M. Ghaffari, and N. Ali, "Comparison of microstructural characteristics and mechanical properties of

shipbuilding steel plates fabricated by conventional rolling versus wire arc additive manufacturing," *Additive Manufacturing*, vol. 32, Article ID 101086, 2020.

[31] V. R. Duarte, T. A. Rodrigues, N. Schell, R. M. Miranda, J. P. Oliveira, and T. G. Santos, "Hot forging wire and arc additive manufacturing (HF-WAAM)," *Additive Manufacturing*, vol. 35, Article ID 101193, 2020.

[32] S. Cadiou, M. Courtois, M. Carin, W. Berckmans, and P. Le masson, "3D heat transfer, fluid flow and electromagnetic model for cold metal transfer wire arc additive manufacturing (Cmt-Waam)," *Additive Manufacturing*, vol. 36, Article ID 101541, 2020.

[33] A. Diourté, F. Bugarin, C. Bordreuil, and S. Segonds, "Continuous three-dimensional path planning (CTPP) for complex thin parts with wire arc additive manufacturing," *Additive Manufacturing*, vol. 37, 2020.

[34] M. Hirtler, A. Jedynak, S. Benjamin, S. Alexander, and M. Bambach, "A study on the mechanical properties of hybrid parts manufactured by forging and wire arc additive manufacturing," *Procedia Manufacturing*, vol. 47, pp. 1141–1148, 2020.

[35] J. Huang, Z. Guan, S. Yu et al., "A 3D dynamic analysis of different depositing processes used in wire arc additive manufacturing," *Materials Today Communications*, vol. 24, Article ID 101255, 2020.

[36] C. Guo, M. Liu, R. Hu et al., "High-strength wire + arc additive manufactured steel," *International Journal of Materials Research*, vol. 111, no. 4, Article ID 1110408, 2020.

[37] C. H. Bharat Kumar and V. Anandakrishnan, "Experimental investigations on the effect of wire arc additive manufacturing process parameters on the layer geometry of Inconel 825," *Materials Today: Proceedings*, vol. 21, no. Pt 1, 2020.

[38] T. A. Rodrigues, V. Duarte, J. A. Avila, T. G. Santos, R. M. Miranda, and J. P. Oliveira, "Wire and arc additive manufacturing of HSLA steel: effect of thermal cycles on microstructure and mechanical properties," *Additive Manufacturing*, vol. 27, pp. 440–450, 2019.

[39] T. Abe and H. Sasahara, "Layer geometry control for the fabrication of lattice structures by wire and arc additive manufacturing," *Additive Manufacturing*, vol. 28, 2019.

[40] C. Dharmendra, A. Hadadzadeh, B. S. Amirkhiz, G. D. Janaki Ram, and M. Mohammadi, "Microstructural evolution and mechanical behavior of nickel aluminum bronze Cu-9Al-4Fe-4Ni-1Mn fabricated through wire-arc additive manufacturing," *Additive Manufacturing*, vol. 30, Article ID 100872, 2019.